Broadband Light Absorption with Multiple Surface Plasmon Polariton Waves Excited at the Interface of a Metallic Grating and Photonic Crystal

Anthony Shoji Hall,[†] Muhammad Faryad,[‡] Greg D. Barber,[†] Liu Liu,[§] Sema Erten,[‡] Theresa S. Mayer,[§] Akhlesh Lakhtakia,[‡,*] and Thomas E. Mallouk[†,*]

[†]Departments of Chemistry, [‡]Engineering Science and Mechanics, and [§]Electrical Engineering, The Pennsylvania State University, University Park, Pennsylvania 16802, United States

ABSTRACT

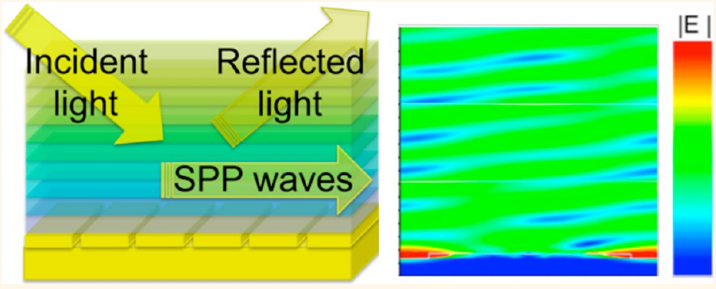

Light incident upon a periodically corrugated metal/dielectric interface can generate surface plasmon polariton (SPP) waves. This effect is used in many sensing applications. Similar metallodielectric nanostructures are used for light trapping in solar cells, but the gains are modest because SPP waves can be excited only at specific angles and with one linear polarization state of incident light. Here we report the optical absorptance of a metallic grating coupled to silicon oxide/oxynitride layers with a periodically varying refractive index, *i.e.*, a 1D photonic crystal. These structures show a dramatic enhancement relative to those employing a homogeneous dielectric material. Multiple SPP waves can be activated, and both s- and p-polarized incident light can be efficiently trapped. Many SPP modes are weakly bound and display field enhancements that extend throughout the dielectric layers. These modes have significantly longer propagation lengths than the single SPP modes excited at the interface of a metallic grating and a uniform dielectric. These results suggest that metallic gratings coupled to photonic crystals could have utility for light trapping in photovoltaics, sensing, and other applications.

KEYWORDS: surface plasmon polariton wave · photonic crystal · metal grating · photovoltaics · broadband light trapping

A one-dimensional (1D) metallic grating is an efficient reflector of light, except when the magnetic field vector of the incident light is parallel to the grating lines and the angle of incidence θ has a particular value. Then, enhanced light absorption arises from the excitation of collective oscillations of conduction electrons near the grating's surface. The coupling generates quasiparticles called surface plasmons that are confined to the vicinity of the metal/air interface. This resonant phenomenon can be analyzed classically in terms of a surface plasmon wave by solving Maxwell's equations for time-harmonic fields. A similar phenomenon occurs when the air above the grating is replaced by a homogeneous, isotropic dielectric material of sufficient thickness. Then the quasiparticles are called surface plasmon polaritons (SPP), and their classical equivalent is the SPP wave.

SPP waves are commonly exploited for sensing[1] and biosensing,[2] optical filtering,[3] and optical data storage.[4] But perhaps their most exciting applications in recent years have been for photovoltaics,[5] photoelectrochemical cells,[6] solar fuel production,[7] and solar thermal photovoltaics.[8] Resonant absorption manifested as the excitation of SPP waves has now been investigated for more

* Address correspondence to axl4@psu.edu, tem5@psu.edu.

Received for review January 22, 2013 and accepted May 25, 2013.

Published online May 26, 2013
10.1021/nn4003488

than three decades as a way of maximizing the conversion of solar light into electricity. It is used in metal grating-backed thin layers of crystalline silicon (~5 μm thick)[9] and amorphous silicon (~0.5 μm thick),[10] which can replace traditionally much thicker (~100 μm) layers of crystalline silicon.

Resonant absorption at the interface of a 1D metallic grating and a homogeneous dielectric material occurs with p-polarized light (*i.e.*, light with its magnetic field vector parallel to the grating lines) but not with s-polarized light (electric field vector parallel to the grating lines).[2,11] Thus, the SPP-wave mode is p-polarized but cannot be s-polarized. The optical energy is confined to a subwavelength thickness in the dielectric material,[5,11,12] and only a single SPP-wave mode can be excited at any given free-space wavelength λ_o over a narrow range of the angle of incidence.[1,11] Hence, the experimental absorptance A ($A = 1 - R - T$, where R and T are the reflectance and transmittance, respectively) of unpolarized broadband light is considerably less than 50% when a 1D metallic grating is employed.[5] To address this problem of polarization sensitivity, light-trapping structures that have angular insensitivity and broadband absorption have been researched in recent years. These structures typically employ two-dimensional (2D) metallic gratings that lower the polarization sensitivity by converting some of the s-polarized light to p-polarized light.[12,17] A strategy to decrease angular sensitivity is to employ metal–insulator–metal (MIM) layers.[14−16] However, MIM structures are highly dissipative because of short SPP wave propagation lengths and large confinement factors.[11] Because of the loss of optical energy within the metal, these structures are of limited use for photovoltaics, which can be efficient only if most of the light is absorbed within the semiconductor.[9,10]

The trapping of light by grating structures can become more efficient if the homogeneous dielectric material is replaced by a periodic multilayer, *i.e.*, a 1D photonic crystal (PC) with a piecewise homogeneous refractive index in the thickness direction. In this case, some recent studies have shown that both incident p- and s-polarized light can excite SPP waves,[18,19] even when the wave vector of the incident light is wholly perpendicular to the grating lines. In these reports, the metal/dielectric interface was planar and a prism-coupled configuration,[20−22] widely used for optical sensing, was employed. Only a *single* p-polarized SPP-wave mode and at most a *single* s-polarized SPP-wave mode were observed experimentally at any λ_o within the photonic band gap of the periodic multilayer. However, a theoretical study on a canonical boundary-value problem has shown that if the dielectric material has a sinusoidally graded refractive index in the thickness direction, then multiple p-polarized and multiple s-polarized SPP-wave modes can be excited at specific wavelengths with high efficiency.[23,24] This prediction

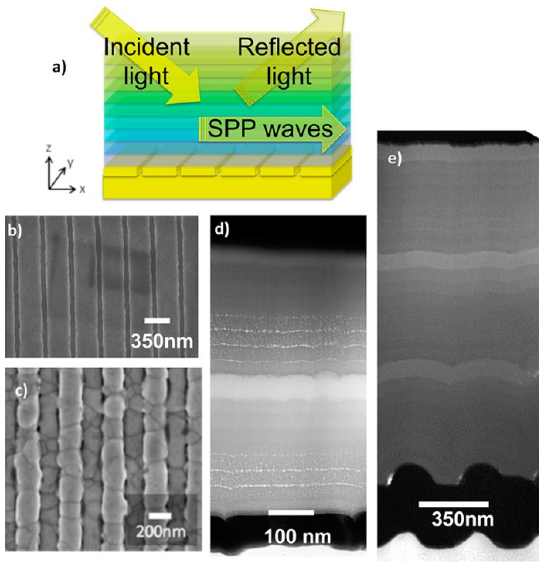

Figure 1. 1D metallic grating coupled to a 1D photonic crystal (periodic multilayer). (a) Schematic of a 1D metallic grating coupled to a multilayer dielectric material, which forms one period of a 1D PC. (b) Top-down SEM image of a gold grating (350 nm period, 80% duty cycle, 50 nm depth). (c) Top-down SEM image of a gold grating (350 nm period, 50% duty cycle, 93 nm depth). (d) Cross-sectional TEM image of a gold grating (350 nm period, 80% duty cycle, 50 nm depth) coupled to a 1D PC with two periods, each consisting of nine layers. (e) Cross-sectional TEM image of a gold grating (350 nm period, 50% duty cycle, 93 nm depth) coupled to a 1D PC with three periods, each consisting of nine layers. The dielectric layers in (d) exhibit some roughness but are quite planar, but those in (e) are quite conformal to the metallic grating. The thickness direction is along the *z*-axis, the grating plane is the *xz*-plane, the grating lines are directed along the *y*-axis, the propagation direction of the incident light lies wholly in the *xz*-plane with the angle of incidence θ measured with respect to the *z*-axis, and SPP waves propagate along the *x*-axis in the *xy*-plane.

was shown theoretically to hold well when the periodic dielectric is backed by a metallic grating,[25] but it has not been experimentally validated.

In this paper, we provide the first experimental evidence that multiple p- and multiple s-polarized SPP-wave modes can be excited over a broad spectral range, in a 1D PC backed by a 1D metallic grating. In our experiments, the wave vector of the incident light was oriented perpendicular to grating lines, so that incident p (respectively s)-polarized light could excite only p (respectively s)-polarized SPP-wave modes. The chosen PC was a nonabsorbing, periodic dielectric material of two or three periods in thickness. Accompanying theoretical results show that many of the SPP-wave modes are weakly localized to the interface of the metal and the PC, display field enhancements that spread throughout the entire two or three periods of the PC, and have very long propagation lengths (on the order of hundreds of micrometers). The latter implies that less energy will be dissipated in the metal when the nonabsorbing dielectric material is replaced by a light absorber, such as the semiconductor layers of a

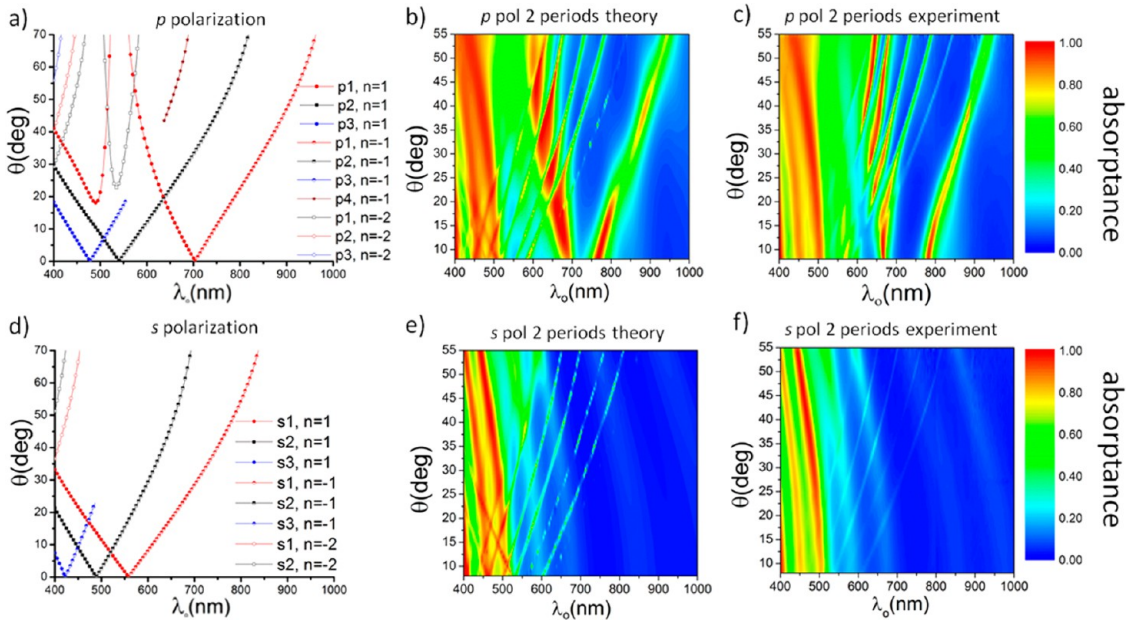

Figure 2. Optical absorptance of a gold grating (350 nm period, 80% duty cycle, 50 nm depth) coupled to a 1D PC. (a, d) Calculated angles of incidence θ for absorptance peaks *vs* free-space wavelength λ_o when either (a) *p*-polarized or (d) *s*-polarized SPP waves are excited. (b, c) Density plots of absorptance as a function of θ and λ_o for incident *p*-polarized light obtained by (b) theory and (c) experiment. (e, f) Density plots of absorptance as a function of θ and λ_o for incident *s*-polarized light obtained by (e) theory and (f) experiment.

photovoltaic cell. Not only SPP-wave modes but also waveguide modes (whose characteristics depend strongly on the thickness of the 1D PC)[25,26] are excited and evidently contribute to broadband absorptance. The efficient coupling of light into these structures has strong implications for performance enhancement of sensors,[1] photovoltaics,[22] and solar thermal photovoltaics.[8]

RESULTS AND DISCUSSION

Fabrication of 1D Grating/Periodic Dielectric Structures. The test structure used in this study is shown schematically in Figure 1a. Here, light is incident from air on a 1D PC that consists of nine different layers in each period and is backed by a 1D metallic grating. The dielectric layer neighboring the grating and filling its troughs is made of silicon nitride (Si_3N_4); the next seven layers are made of silicon oxynitride $\{(Si_3N_4)_a(SiO_2)_{1-a}\}$, each with a different value of a; and the ninth (top) layer is made of silicon oxide (SiO_2). Figure SI-1 gives the measured refractive indexes of all nine dielectric materials as functions of λ_o. The imaginary part of the refractive index was below 10^{-4} in the spectral regime studied for all the dielectric materials, and it was therefore ignored in the calculations.

Top-down scanning electron microscope (SEM) images and cross-sectional transmission electron microscope (TEM) images of structures fabricated and characterized in this study are shown in Figure 1b–e. Whereas the vapor-deposited dielectric layers in the shallow grating structure shown in Figure 1d appear more or less planar, those shown in Figure 1e, which is a structure with a deeper metallic grating, are more conformal.

Due to the periodicity of the metallic grating, the Bloch theorem[27,28] mandates that the reflected and the transmitted fields must contain both specular and nonspecular components when the structure is illuminated by a monochromatic plane wave. Furthermore, the fields induced inside the structure must consist of Floquet harmonics of negative, zero, and positive orders.[29] It is the panoply of Fourier harmonics that facilitates the excitation of multiple SPP-wave modes in the grating-coupled configuration under investigation.[30−32] Because the metallic gratings are ~200 nm thick, they do not transmit light in the wavelength range studied and hence $T = 0$ in all experiments.

Calculations of the reflected field were made for $0° \le \theta \le 70°$ (where 0° is defined as normal incidence) for λ_o between 400 and 1000 nm using the rigorous coupled wave approach.[25,29] The measured complex refractive index of gold, shown in Figure SI-2, was used in the calculations along with the data in Figure SI-1 for the dielectric materials. Over most of the $\theta \times \lambda_o$ domain chosen for the calculations and for incident light of both p- and s-polarization states, the nonspecular reflected components were very weak for the structure that has a shallow grating (Figure 1d), as can be deduced from comparing Figures 2 and SI-3. Accordingly, only the specular reflectances R_{0p} and R_{0s} were measured at angles between 8° and 55° in order to determine the absorptances $A_p \approx 1 - R_{0p}$ and $A_s \approx 1 - R_{0s}$. We calculated absorptances for the structure shown in Figure 1d when the PC contained either

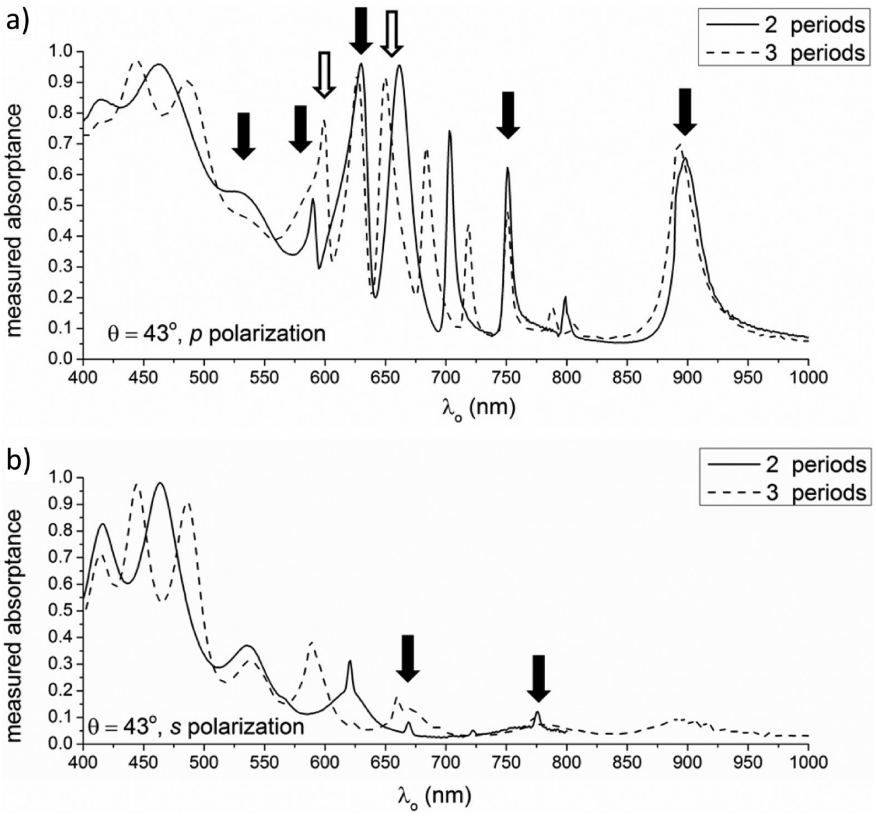

Figure 3. Measured optical absorptance of a gold grating (350 nm period, 80% duty cycle, 50 nm depth) coupled to a 1D PC at $\theta = 43^\circ$. (a, b) Measured absorptance as a function of λ_o when $\theta = 43^\circ$ for incident (a) p-polarized light and (b) s-polarized light. The 1D PC has either two (solid lines) or three (dashed lines) periods. Downward arrows denote the absorptance peaks that correspond to the excitation of SPP-wave modes.

two or three periods. Peaks in the plots of A_p and A_s *vs* θ (respectively λ_o) for fixed λ_o (respectively θ) were identified. Each absorptance peak whose λ_o location (at a fixed θ) or θ location (at a fixed λ_o) depended very weakly on the number of periods of the PC beyond a threshold indicated the excitation of an SPP-wave mode, which we then confirmed by the solution of a canonical boundary-value problem.[21,27] At a fixed λ_o, we also determined the order n of the Floquet harmonic corresponding to each excited SPP-wave mode from the canonical boundary-value problem.[25,31]

Excitation of Multiple SPP Waves in Shallow 1D Grating Structures. Figure 2 compares experimental and theoretical results for a gold metallic grating with a period of 350 and 50 nm tall rectangular raised sections that span 80% (duty cycle) of each period. The metallic grating is shown alone in Figure 1b, and the entire structure comprising the grating and the PC is shown in cross-section in Figure 1d. Figure 2a and d show the calculated θ locations and λ_o locations of p- and s-polarized SPP-wave modes for λ_o between 400 and 1000 nm.[21,27] As many as 10 p- and eight s-polarized SPP-wave modes are theoretically possible for this structure. Density plots of theoretically predicted and experimentally measured absorptances as functions of θ and λ_o are presented in Figure 2b,c and 2e,f for incident p- and s-polarized light, respectively, for the two-period PC backed by the grating.

The loci of absorptance peaks in the contour plots in Figure 2b,c closely resemble the lines in Figure 2a, and the same statement can be made for Figure 2e,f and 2d. Remarkably, the experimental data confirm the existence of nine of 10 p-polarized SPP-wave modes predicted theoretically. All four modes identified by $n = -1$, two of three modes identified by $n = +1$, and one of three modes identified by $n = -2$ in Figure 2a are clearly evident in Figure 2c. The existence of the two other modes identified by $n = -2$ in Figure 2a can be discerned experimentally in a high-resolution version of Figure 2c, but their excitation is weak because of the strong background absorption at $\lambda_o < 500$ nm caused by waveguide modes superimposed on the interband transitions of gold.[11] The onset of gold's interband transitions lies below $\lambda_o < 600$ nm, but the transitions do not completely dominate the signal until $\lambda_o < 500$. In contrast, the experimental data confirm the existence of only two of eight s-polarized SPP-wave modes. Both of these modes are identified by $n = -1$ in Figure 2f. Both theory and experiment indicate that s-polarized SPP-wave modes are excited weakly in comparison to the p-polarized SPP-wave modes in the structure of Figure 1d. This suggests that this structure is not very efficient in using incident

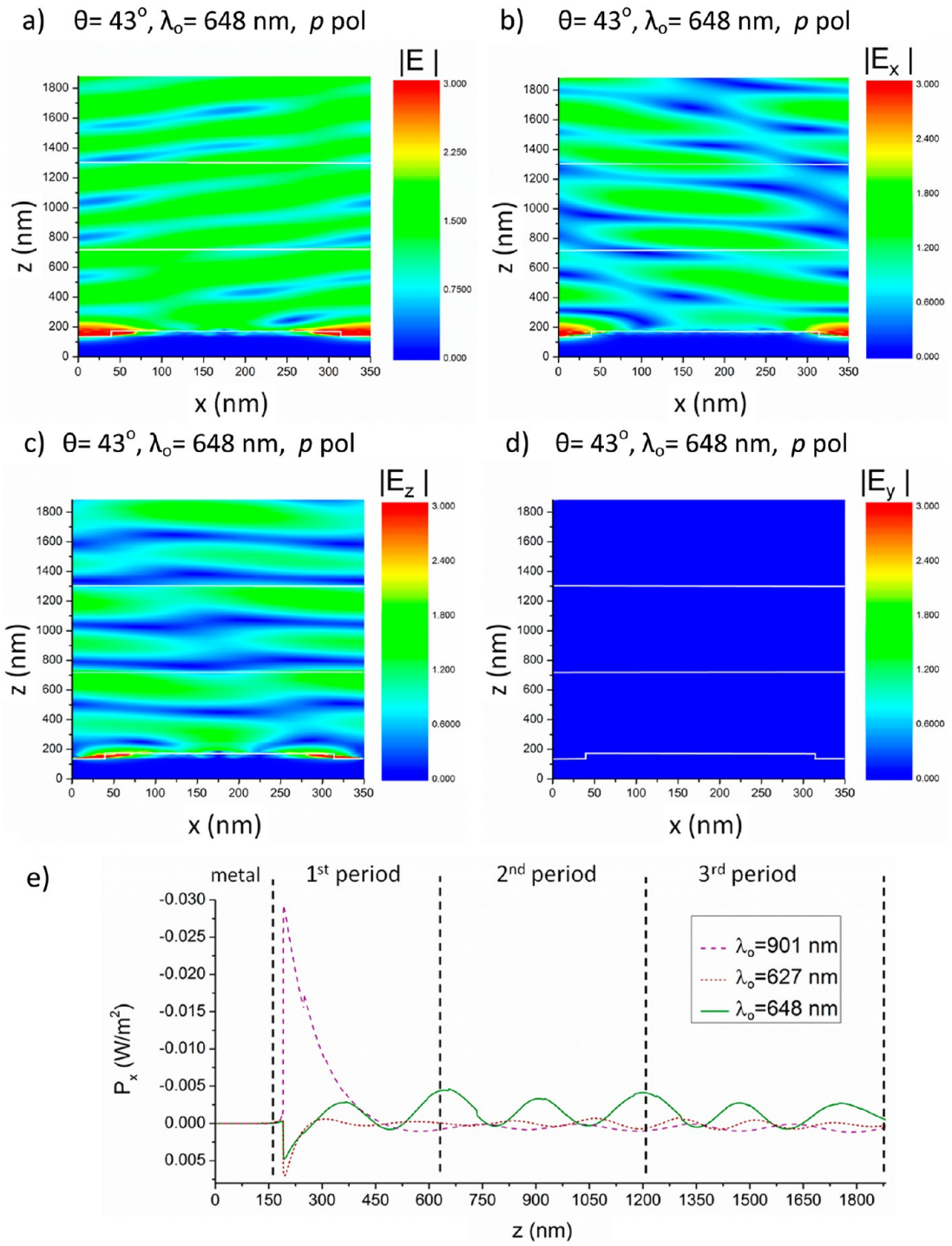

Figure 4. Field profiles of p-polarized SPP-wave modes for a gold grating (350 nm period, 80% duty cycle, 50 nm depth) coupled to a 1D PC. (a–d) Contour plots of magnitudes of (a) the electric field, (b) the *x*-component of the electric field, (c) the *z*-component of the electric field, and (d) the *y*-component of the electric field, calculated as functions of *x* and *z* when λ_o = 648 nm, θ = 43°, and an SPP-wave mode is excited by incident p-polarized light. (e) Calculated variation of the *x*-directed component of the time-averaged Poynting vector along the *z*-axis at *x* = 175 nm (*i.e.*, in the *xz*-plane bifurcating a protrusion) for θ = 43° at λ_o = 901, 627, and 648 nm when p-polarized incident light excites an SPP-wave mode. The dashed lines in (e) denote either the mean metal/dielectric interface or the end of a period of the PC. All calculations were made for an incident plane wave with an electric field of amplitude 1 V/m.

s-polarized light to excite SPP-wave modes. This conclusion holds even when the number of periods of the PC is increased from two to three, as can be seen by comparing the density plots in Figure 2b,c, e,f (two periods) with their counterparts in Figure SI-4 (three periods).

Differentiating p- and s-Polarized SPP Modes from Waveguide Modes. To provide greater clarity about the excitation

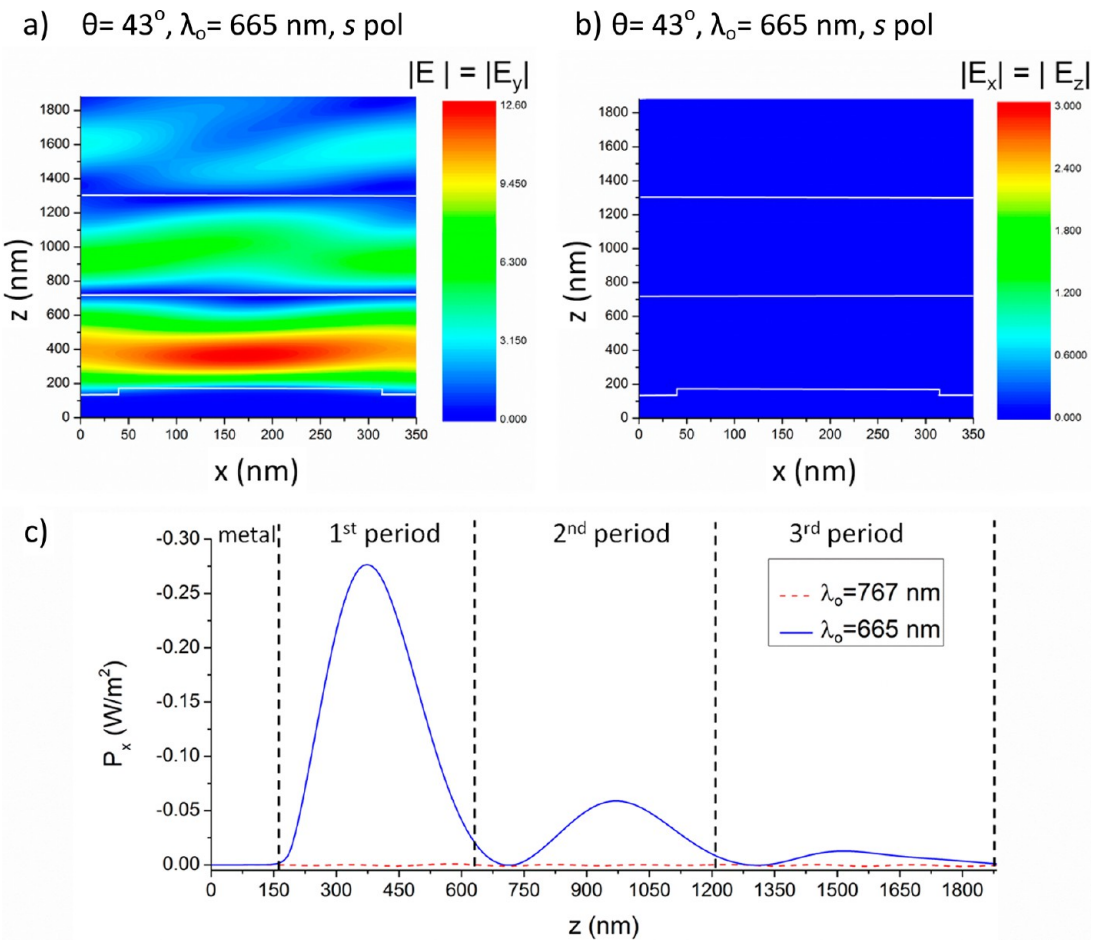

Figure 5. Field profiles of s-polarized SPP-wave modes for a gold grating (350 nm period, 80% duty cycle, 50 nm depth) coupled to a 1D PC. (a, b) Contour plots of the magnitude of (a) the electric field (the *y*-component of the electric field) and (b) the *x*-component (or *z*-component) of the electric field. (c) Calculated variation of the *x*-directed component of the time-averaged Poynting vector along the *z*-axis at $x = 175$ nm (*i.e.*, in the *xz*-plane bifurcating a protrusion) for $\theta = 43°$ at $\lambda_o = 767$ and 665 nm when s-polarized incident light excites an SPP-wave mode. The dashed lines in (c) denote either the mean metal/dielectric interface or the end of a period of the PC. All calculations were made for an incident plane wave with an electric field of amplitude 1 V/m.

of multiple SPP-wave modes with respect to the number of periods in the PC, experimentally measured and theoretically predicted absorptances are presented as functions of λ_o for $\theta = 43°$. These absorptances are shown for two- and three-period PCs in Figures 3 and SI-5, respectively. Every absorptance peak whose θ location at fixed λ_o remains invariant with the addition of the third period of the photonic crystal definitely corresponds to the excitation of SPP-wave modes. Conversely, the peaks whose θ-values are highly sensitive to the total thickness of the PC are waveguide modes.[25] The energy of an SPP-wave mode is localized, weakly or strongly, to the metal/dielectric interface, but the energy of a waveguide mode is more evenly distributed throughout the thickness of the dielectric layers. Downward arrows in Figures 3a and SI-5a identify five p-polarized SPP-wave modes for $\lambda_o > 500$ nm. The interband transitions of gold[11] prevent the resolution of SPP-wave modes at wavelengths shorter than 500 nm. The broad peak at $\lambda_o = 520$ nm corresponds to the excitation of two co-propagating SPP-wave modes as Floquet harmonics of orders $n = 1$ and $n = -2$. For the purpose of comparison, the measured absorptance of a flat gold film with two or three periods of the PC is presented in Figure SI-6. No invariant peaks are observed, because only waveguide modes can be excited when the grating is absent. Furthermore, the absorptance of this control sample is nearly null for both polarization states for $\lambda_o > 600$ nm, indicating that the PC or Fabry–Perot interference modes do not give rise to significant absorption of light at wavelengths longer than the interband transitions of gold.

Inspection of Figures 3 and SI-5 reveals that some SPP-wave modes shift slightly with the addition of a third period to the PC. In Figure 3a, we observe an SPP-wave mode in the vicinity of $\lambda_o \approx 600$ nm that is not evident unless three periods of the PC are present above the metallic grating. Furthermore, in the same figure we observe a significant shift of an SPP-wave mode from $\lambda_o = 660$ nm to $\lambda_o = 648$ nm when the

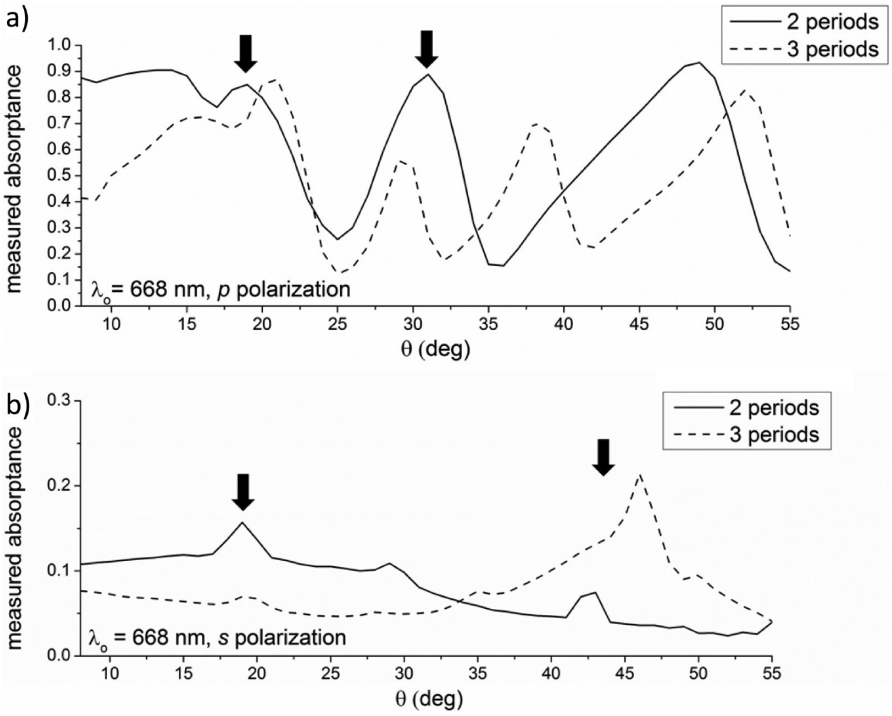

Figure 6. Measured optical absorptance of a gold grating (350 nm period, 80% duty cycle, 50 nm depth) coupled to a 1D PC at λ_o = 668 nm. (a, b) Measured absorptance as a function of θ when λ_o = 668 nm for incident (a) p-polarized light or (b) s-polarized light. The 1D PC has either two (solid lines) or three (dashed lines) periods. Downward arrows denote the absorptance peaks that correspond to the excitation of SPP-wave modes.

thickness of the PC is increased from two to three periods. These SPP-wave modes, denoted by open arrows in Figure 3, are weakly localized to the metal/dielectric interface and, therefore, are highly sensitive to the dielectric environment above the metallic grating. Figure 4a–d show the calculated spatial profiles of the magnitudes of the components of the electric field. It is evident that the SPP-wave modes excited with p-polarized light do not contain any electric field oriented parallel to the *y*-direction; therefore SPP waves excited with p-polarized light are completely p-polarized in nature. Although the contour plots show that the electric field strength is maximized near the corners of the metallic grating, a significant portion of the field extends into all three periods of the dielectric stack. Figure 4e shows the variation along the thickness direction (*z*-axis) of the component of the time-averaged Poynting vector in the direction of propagation, taken at a slice through the middle of the grating (x = 175 nm, *x*-axis) for the SPP-wave modes at λ_o = 648, 627, and 901 nm for the three-period PC. The SPP-wave modes at λ_o = 627 and 901 nm are localized to the metal/dielectric interface, decaying within ~270 and ~75 nm, respectively, into the first period of the PC. These modes shift only slightly when the number of periods of the PC is increased from two to three, consistent with their localization to the metal/PC interface. In contrast, the SPP-wave mode at λ_o = 648 nm exhibits a large shift because its Poynting vector is distributed into all three layers of the PC.

The absorptance peaks identified by downward arrows in Figures 3b and SI-6b indicate the excitation of two different s-polarized SPP-wave modes at $\theta = 43°$. An SPP-wave mode in Figure 3b at λ_o = 660 nm when the PC has two periods blue-shifts to λ_o = 655 nm with the addition of a third period. From Figure 5b, it is clear that this SPP-wave mode is completely s-polarized since its E_x and E_z components are zero. Figure 5c presents the variation along *z* of the *x*-directed component of the time-averaged Poynting vector of this SPP-wave mode and an SPP-wave mode at λ_o = 665 nm for the three-period structure. As expected from the significant blue shift, this SPP-wave mode is weakly localized to the metal/dielectric interface. The electric field has a maximum magnitude not in the mean plane of the periodically corrugated metal/dielectric interface but in the middle of the first period of the dielectric. This characteristic is very different from that of the p-polarized SPP-wave modes in Figure 4c. The *x*-directed component of the time-averaged Poynting vector of the SPP-wave mode at λ_o = 767 nm is very small because it is weakly excited.

Each panel in Figure 2 shows that different SPP-wave modes can be excited at a single λ_o by light incident at different angles. For instance, when λ_o = 668 nm, two p- and two s-polarized SPP-wave modes are excited, as shown in Figure 6. Corresponding plots of calculated absorptances are shown in Figure SI-7. These SPP-wave modes differ in phase speed $v_p = c/[(n\lambda_o/L) + \sin\theta]$, where L is the period of the

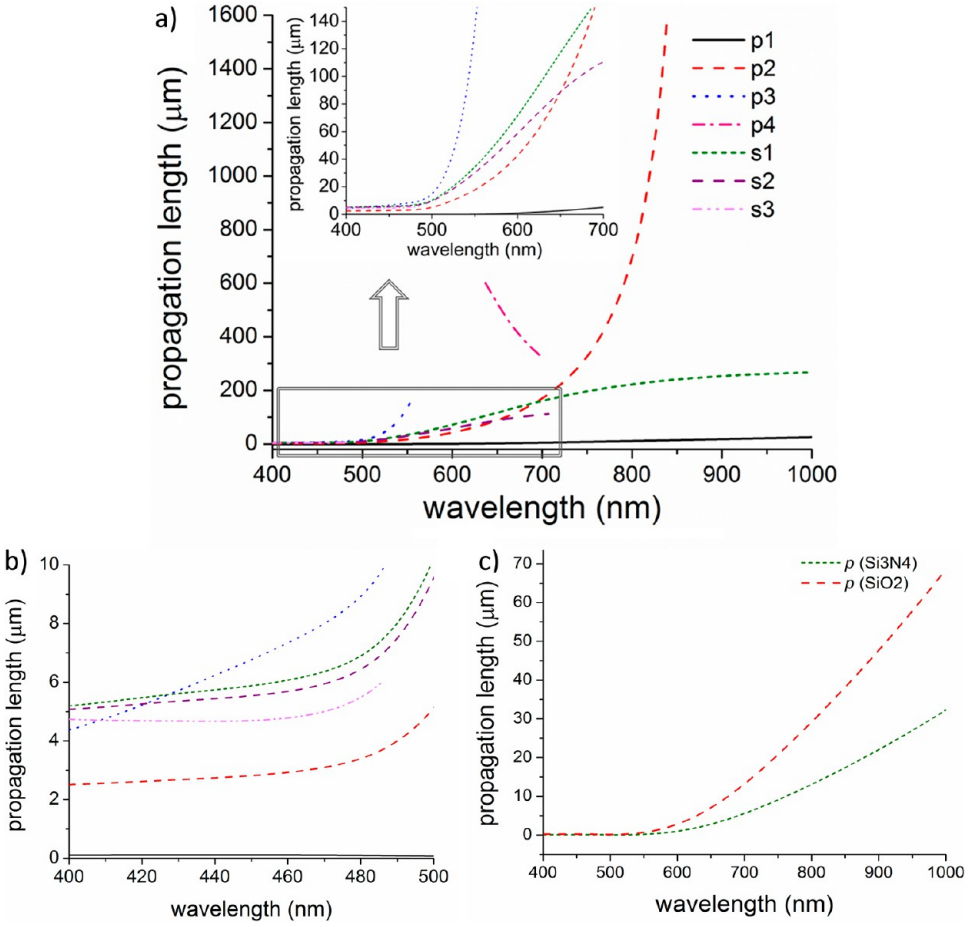

Figure 7. Calculated propagation lengths of SPP waves. (a) Calculated propagation lengths of p- and s-polarized SPP waves excited at the interface of a shallow 1D gold grating (350 nm period, 80% duty cycle, 50 nm depth) and a 1D PC. Inset shows an expanded view of the boxed region. (b) Expanded view of (a) showing the propagation lengths of SPP-wave modes for $\lambda_o < 500$ nm. (c) Propagation lengths of SPP-wave modes when the PC layers are replaced by a uniform slab of silicon nitride or silicon dioxide.

grating, as they are excited at different angles of incidence as Floquet modes of different orders n, c being the speed of light in free space. An increase in the number of periods in the PC can cause a small increase or decrease in θ for the excitation of a certain SPP-wave mode, but that value of θ stabilizes after the number of periods crosses a threshold, according to theoretical data shown in a previous paper.[20]

Propagation Lengths of SPP Waves. In the simple test structures investigated in this study, any light that is not reflected must be absorbed because the metal grating is very thick. Because the dielectric material is nonabsorbing, all of the absorption therefore takes place in the gold gratings. However, in real applications in which the dielectric material absorbs light, the SPP wave propagation length is an important figure of merit. Longer propagation lengths imply that a greater fraction of trapped light will be absorbed in the absorbing dielectric layers rather then in the metal. Figure 7a shows the calculated propagation lengths of the multiple p- and s-polarized SPP waves excited in the structure shown in Figure 1d. The labeling of the SPP waves is the same as in Figure 2a,d to allow easy comparison of the propagation lengths of the SPP-wave modes. One of the p-polarized SPP-wave modes, denoted as p2, has a propagation length of 1500 μm (1.5 mm) at $\lambda_o = 800$ nm. Most of the other p-polarized SPP-wave modes have propagation lengths that are 100 μm or longer when $\lambda_o > 600$ nm. The SPP wave modes of branches p2−p5 have very short propagation lengths for $\lambda_o < 600$ nm. However, when $\lambda_o > 600$ nm these modes can have propagation lengths greater than 100 μm. Due to the low propagation length of the p1 SPP mode over the entire spectral range, this SPP mode must be highly confined to the metal/dielectric interface. Two of the s-polarized SPP modes, denoted as s1 and s2, have propagation lengths of 80 μm or longer when $\lambda_o > 600$ nm. The other s-polarized SPP mode, denoted as s3 in Figure 7, is excited below $\lambda_o < 490$ nm; the propagation length of this mode is short (~4.8 μm) because of strong absorption of light by gold in the region of the interband transitions. Figure 7b shows that the propagation lengths of all the SPP-wave modes converge to 2−5 μm for $\lambda_o < 500$ nm

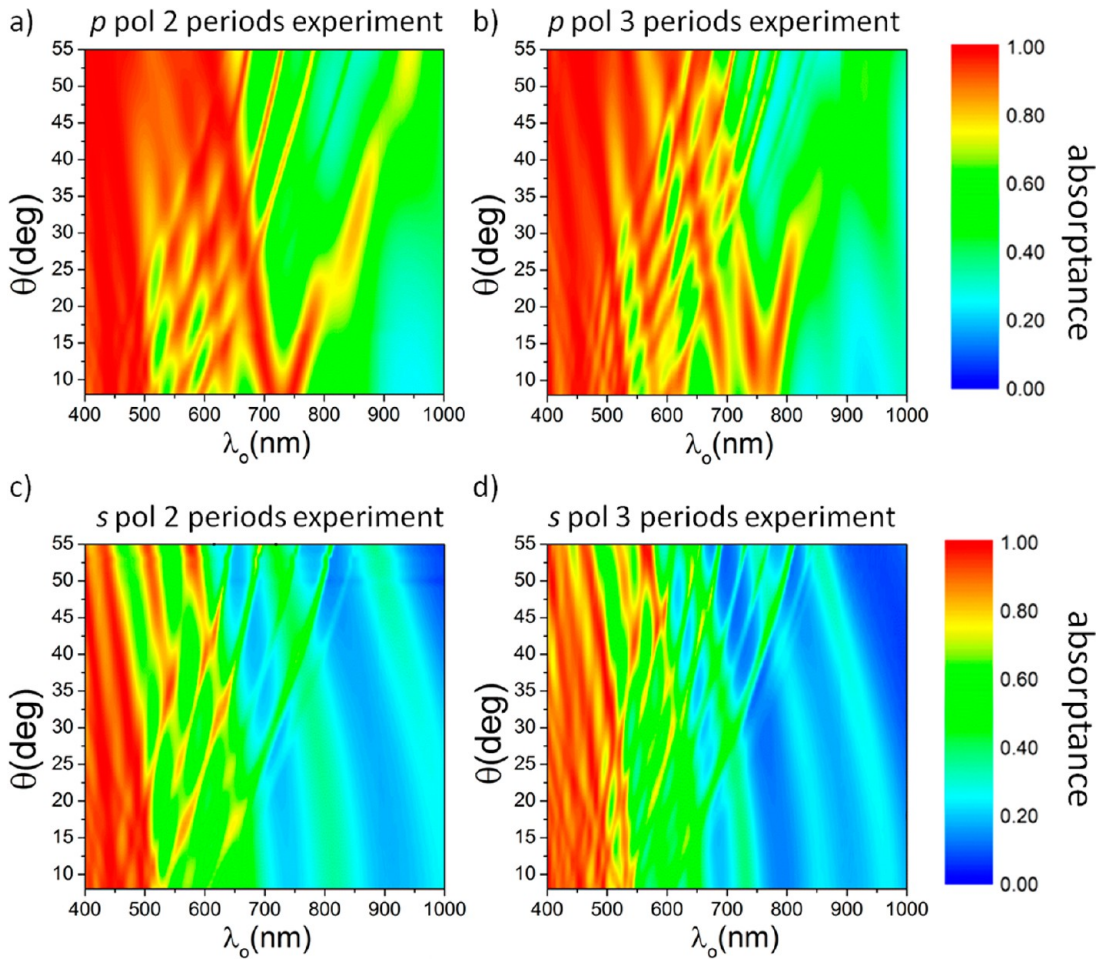

Figure 8. Measured optical absorptance of a gold grating (350 nm period, 50% duty cycle, 93 nm depth) coupled to a 1D PC. (a, b) Density plots of measured absorptance as a function of θ and λ_o for incident p-polarized light when the 1D PC has either (a) two or (b) three periods. (c, d) Density plots of measured absorptance as a function of θ and λ_o for incident s-polarized light when the 1D PC has either (c) two or (d) three periods.

because of this effect; an expanded view of this region is shown in Figure 7b. Figure 7c shows the propagation lengths for a structure in which the PC is replaced by a uniform slab of silicon oxide or silicon nitride. In this case, the propagation lengths are shorter than 100 μm across the entire spectral range of interest. The important conclusion is that multiple SPP modes generated in the PC can propagate farther because light is not, in general, as strongly localized to the metal/dielectric interface as it is in uniform dielectric structures.

Excitation of s- and p-Polarized SPP Waves in Deep 1D Grating Structures. The experimental and theoretical results described heretofore establish the broadband excitation of multiple SPP-wave modes using both p- and s-polarized light, but the latter modes are quite weak and are therefore of limited utility for light trapping in the dielectric layers. In order to improve the excitation efficiency of the s-polarized SPP-wave modes, we redesigned the gold grating to have 93 nm depth and 50% duty cycle, keeping the grating period L still fixed at 350 nm (Figure 1c). When the PC was deposited on this grating, the dielectric layers conformed to the grating's corrugations, as shown in Figure 1e for a three-period PC.

The redesigned grating yields stronger excitation of both s- and p-polarized SPP-wave modes and waveguide modes, according to the density plots shown in Figure 8 for two- and three-period structures. SPP-wave modes of either polarization state that are excited as Floquet harmonics with $n > 0$ are now excited with higher efficiency than in Figure 2, even in the spectral regime of high background absorption due to the interband transitions of gold. Modes that are excited at $\lambda_o < 600$ nm as Floquet harmonic of the order $n = -1$ are overestimated by 5−15% when $\theta > 40°$ due to nonspecular reflection (Figure SI-8). The optical response of this structure is very sensitive to the dielectric profile above the metallic grating. Reliable comparisons with theoretical predictions from the rigorous coupled wave approach[25,29] could not be accomplished for the deeper grating structure because the calculations are sensitive to several inputs: (i) the curves describing the shape of each conformal dielectric layer, (ii) variations in the thickness and the

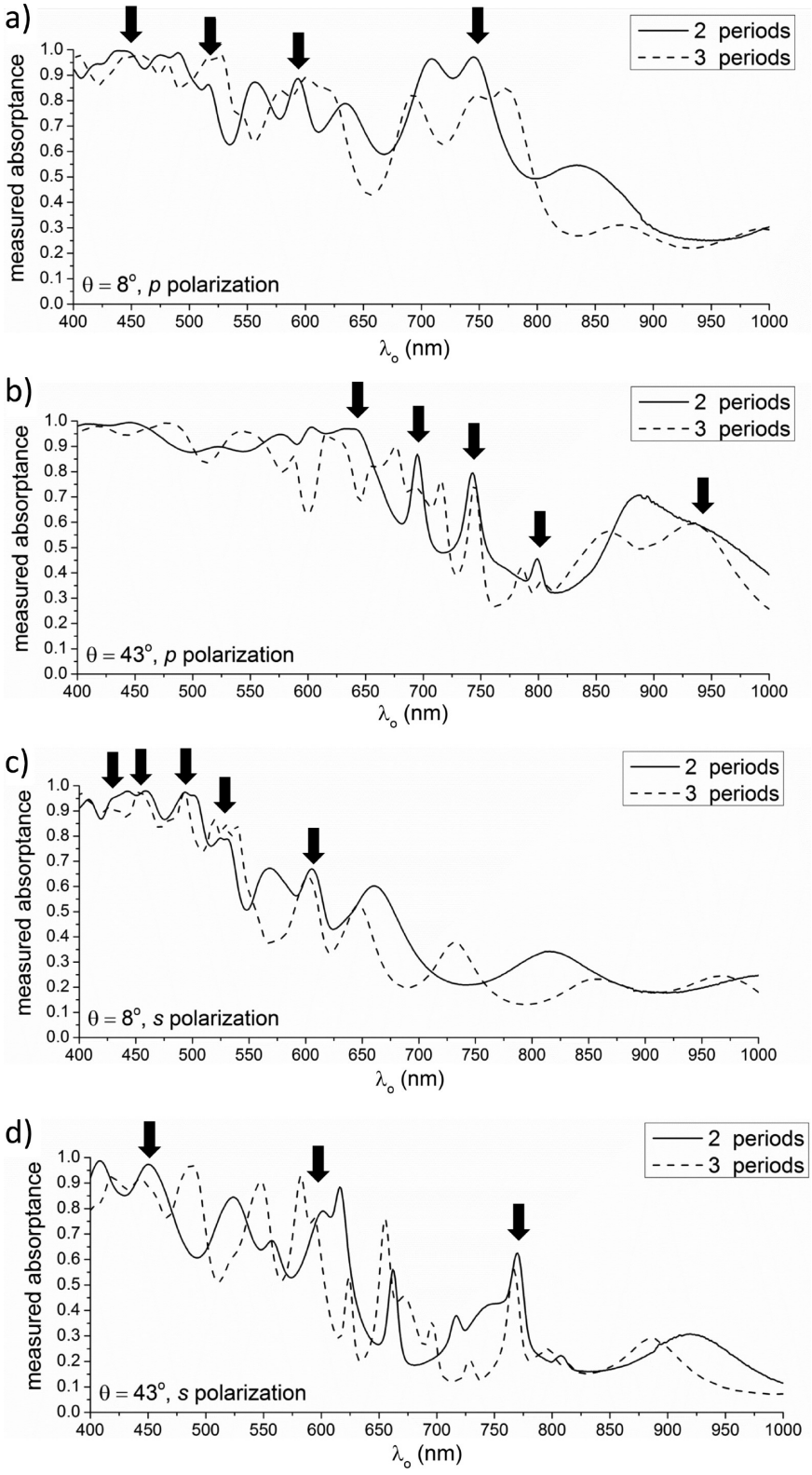

Figure 9. Measured optical absorptance of a gold grating (350 nm period, 50% duty cycle, 93 nm depth) coupled to a 1D PC. (a, b) Measured absorptance as a function of λ_o for incident p-polarized light, when θ is either (a) 8° or (b) 43°. (c, d) Measured absorptance as a function of λ_o for incident s-polarized light, when θ is either (c) 8° or (d) 43°. The 1D PC has either two (solid lines) or three (dashed lines) periods. Downward arrows denote the absorptance peaks that correspond to the excitation of SPP-wave modes.

composition of each dielectric layer from one unit cell to another, and (iii) the aperiodicity of the corrugations of the metallic grating. A more realistic model would require several unit cells of the structure to be treated

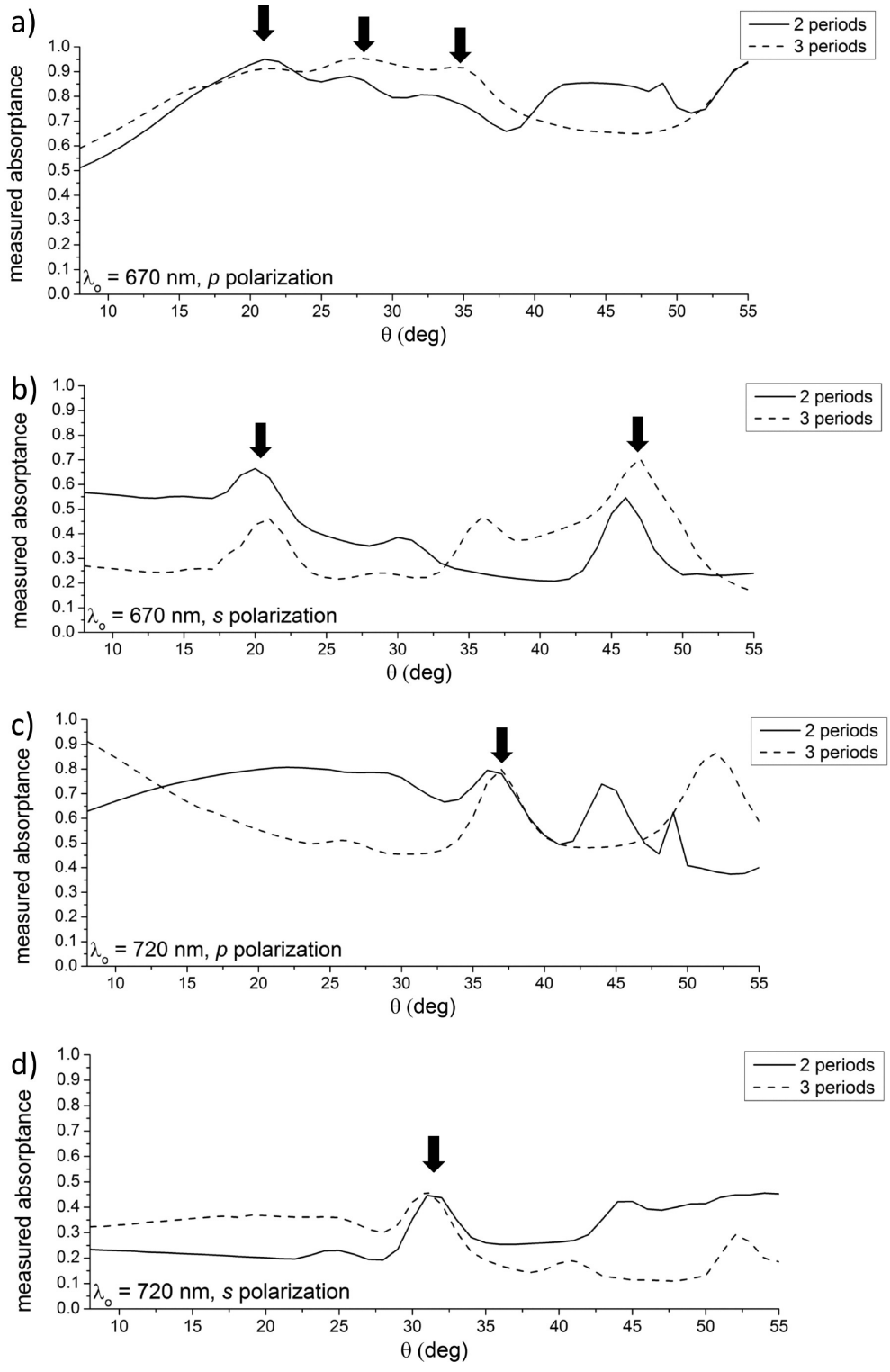

Figure 10. Optical absorptance of a gold grating (350 nm period, 50% duty cycle, 93 nm depth) coupled to a 1D PC. (a, b) Measured absorptance as a function of θ when λ_o = 670 nm and the incident light is either (a) p or (a) s polarized. (c, d) Measured absorptance as a function of θ when λ_o = 720 nm and the incident light is either (c) p or (d) s polarized. The 1D PC has either two (solid lines) or three (dashed lines) periods. Downward arrows denote the absorptance peaks that are likely to correspond to the excitation of SPP-wave modes.

as one unit cell, but then computations could not be made within a reasonable period of time. These difficulties notwithstanding, theoretical contour plots for samples with two periods of the PC, calculated on the basis of the simple unit cell, are presented in Figure SI-9.

Figure 9 shows the measured absorptances A_p and A_s as functions of λ_o for $\theta = 8°$ and $\theta = 43°$ for two- and

three-period PC structures. Similar plots, but as functions of θ for λ_o = 670 nm and λ_o = 720 nm, are provided in Figure 10. Four p-polarized SPP-wave modes and five s-polarized SPP-wave modes are excited at θ = 8°; likewise, five p-polarized and three s-polarized SPP-wave modes are excited at θ = 43°. More p-polarized SPP-wave modes are excited at higher θ, but more s-polarized SPP modes are excited at lower θ.

Figure 10 shows that two p- and two s-polarized SPP-wave modes are excited at λ_o = 670 nm, but only one SPP-wave mode of each polarization state is excited at λ_o = 720 nm. The excitation efficiencies of the s-polarized SPP-wave modes are higher at lower λ_o. Importantly, while the excitation efficiencies of the s-polarized SPP-wave modes are not as high as those of the p-polarized SPP-wave modes, they are clearly much higher than those of the s-polarized SPP-wave modes in the shallow grating structure shown in Figure 1d. Indeed, we conclude from Figures 8, 9, and 10 that the excitation efficiencies of s-polarized SPP-wave modes in the deeper grating structure of Figure 1e can approach 100% (*i.e.*, $A_s \approx 1.0$). It is also likely that the redesigned structure supports more SPP-wave modes than identified in these figures. The weakly bound SPP-wave modes that are not invariant with the PC thickness require more accurate theoretical modeling to confirm their existence.

CONCLUSIONS

We have theoretically modeled and experimentally demonstrated a new approach for broadband trapping of light as SPP-wave modes: an appropriately designed metallic-grating-backed periodic dielectric multilayer supports the existence of *multiple* SPP-wave modes[33] of both p- and s-polarization states over a wide spectrum of free-space wavelengths. Significantly, we have successfully demonstrated that with proper design s-polarized SPP-wave modes can be excited with high efficiency.

Solution of the time-harmonic Maxwell equations indicates that the fields of several SPP-wave modes are weakly localized to the periodically corrugated metal/dielectric interface. The weakness of the localization implies that the incident light energy can be more evenly distributed in a light-absorbing PC that is the active component of a sensor or solar cell. The long propagation lengths of many of the multiple SPP waves also indicate that less energy is dissipated in the metallic layer relative to structures with uniform dielectrics. Theory shows that the relationship between the number of SPP-wave modes that can be excited in a given spectral regime and the period of the PC is somewhat complicated.[24] In this initial experimental study, we found that multiple SPP-wave modes are excited in a range of free-space wavelengths λ_o comparable to the period of the PC. This effect remains to be explored and optimized for specific applications.

The materials used in this study are commonplace in nanotechnology. Given the broad interest in plasmonic nanostructures and photonic crystals, which can be fabricated from many different materials, the synergy that arises from their combination should be useful in many future optical applications.

MATERIALS AND METHODS

Fabrication of Metallic Gratings. Metallic gratings were fabricated as described in detail elsewhere.[34] In brief, silicon wafers were patterned by electron beam lithography on ZEP520A photoresist (Zeon, Tokyo) with the inverse pattern of the desired metallic grating. The pattern in the photoresist was transferred into the silicon by inductively coupled reactive ion etching on a Versalock 700 (Plasma-Therm, St. Petersburg, FL, USA) with pure Cl_2 gas. The photoresist dissolved in Nanostrip, a commercially available resist remover, with the assistance of a bath sonicator. Gold was thermally evaporated on the patterned silicon wafer at room temperature with a base pressure of $<1 \times 10^{-6}$ at 0.1 nm/s. The gold film was attached to a glass slide using EpoTek 377 epoxy (Epoxy Technology, Billerica, MA, USA). The epoxy resin was cured by a seven-day thermal treatment at 125 °C. The gold film was released from the silicon wafer with a razor blade, yielding a gold grating glued to a glass slide. All gratings used in this work were 6 × 6 mm in size.

Fabrication of Periodic Dielectric Multilayers. Periodic multilayers of silicon oxide/oxynitride were grown directly on the gold gratings by plasma-enhanced chemical vapor deposition on a Cluster Tool (Applied Materials, Santa Clara, CA, USA) at a susceptor temperature of 220 °C. Ammonia, silane, and nitrous oxide were used in varying ratios to deposit layers with specific refractive indices. All layers were deposited at a pressure of 3.5 Torr and a power density of 0.955 W/cm^2.

Electron Microscopy. SEM images were collected on a Leo 1530 FESEM (Carl Zeiss, Oberkochen, Germany), and TEM images were collected on a Phillips 420 TEM (Phillips, Amsterdam, The Netherlands).

Optical Characterization of Dielectric and Gold Layers. The complex refractive index of each layer, whether dielectric or metallic, was calculated from data obtained by using an RC2 spectroscopic ellipsometer (Woollam, Lincoln, NE, USA). For these measurements, a thin film of the same nominal thickness and composition as those grown for the multilayer structures (Figure 1) was deposited under identical conditions on a glass slide or silicon wafer. The spot size used for collection of the data was 3.5 × 3.5 mm.

Parameters for Theoretical Simulations. For computation of absorptances using the rigorous coupled wave approach of the structure containing gold gratings of 350 nm period, 80% duty cycle, and 50 nm depth, the unit cell profile of the gratings was approximated by a sinusoid, as suggested by cross-sectional views (not presented) of the grating shown in Figure 1b. The grating region was divided into 2 nm thick slices parallel to the mean plane of the metal/dielectric interface, and each slice was considered to be homogeneous. For computations, 31 Floquet harmonics were used.

Measurements of Specular and Nonspecular Reflectances. Specular reflectance measurements were performed on a Lambda 950 UV−visible spectrometer (Perkin-Elmer, Waltham, MA, USA) with a Universal Reflectance accessory. Measurements were performed in steps of 1 nm for λ_o and 1° for θ. The nonspecular reflectance of order −1 was measured using a dual rotary stage arrangement. Monochromatic light, in 5 nm intervals, was selected from a broadband source (150 W Xe arc lamp, Oriel-Newport) through a single pass monochromator. The intensity of the

monochromatic beam was determined from the specular reflectance from a calibrated silver mirror in place of the grating and a silicon photodiode (Hamamatsu Corporation, S1226-44BQ, 3.6 mm × 3.6 mm) at a nominal distance of 110 mm from the mirror/grating plane. At this distance, the silicon photodiode detector occupies a subtended angle of approximately 1.9°. The intensity of the nonspecular, −1 order reflected light was measured using the same silicon photodiode. The intensity of the nonspecularly reflected light was obtained from the ratio of the grating-detector current to the calibrated current measured from the Ag mirror.

Conflict of Interest: The authors declare no competing financial interest.

Acknowledgment. We thank Trevor Clark, Josh Maier, and Dimitri Vaughn for assistance with transmission electron microscopy. We also gratefully acknowledge helpful discussions with Peter Monk and Manuel Solano. This work was supported by the National Science Foundation under grant no. DMR-1125591. Fabrication experiments were performed at the Pennsylvania State University Materials Research Institute Nanofabrication Laboratory, which is supported by the National Science Foundation under Cooperative Agreement No. ECS-0335765. A.L. is also grateful to Charles Godfrey Binder Endowment at the Pennsylvania State University for partial support of this work.

Supporting Information Available: Definition of a surface plasmon polariton wave, refractive index *vs* wavelength data for metal and dielectric layers, nonspecular reflectance data, reflectance data for three-period photonic crystals on gold gratings, calculated absorptance spectra for two- and three-period photonic crystals on shallow gold gratings, experimental absorptance spectra for photonic crystals on flat gold substrates, and absorptance spectra of photonic crystals on deep gold gratings. This material is available free of charge *via* the Internet at http://pubs.acs.org.

REFERENCES AND NOTES

1. Homola, J.; Yee, S. S.; Gauglitz, G. Surface Plasmon Resonance Sensors: Review. *Sens. Actuators, B* **1999**, *54*, 3–15.
2. Abdulhalim, I.; Zourob, M.; Lakhtakia, A. Surface Plasmon Resonance for Biosensing: A Mini-Review. *Electromagnetics* **2008**, *28*, 214–242.
3. Dandin, M.; Abshire, P.; Smela, E. Optical Filtering Technologies for Integrated Fluorescence Sensors. *Lab Chip* **2007**, *7*, 955–977.
4. Zia, R.; Selker, M. D.; Catrysse, P. B.; Brongersma, M. L. Geometries and Materials for Subwavelength Surface Plasmon Modes. *J. Opt. Soc. Am. A* **2004**, *21*, 2442–2446.
5. Atwater, H. A.; Polman, A. A. Plasmonics for Improved Photovoltaic Devices. *Nat. Mater.* **2010**, *9*, 205–213.
6. Nishijima, Y.; Nishijima, Y.; Ueno, K.; Kotake, Y.; Murakoshi, K.; Inoue, H. Misawa. Near-Infrared Plasmon-Assisted Water Oxidation. *J. Phys. Chem. Lett.* **2012**, *3*, 1248–1252.
7. Ingram, D. B.; Linic, S. Water Splitting on Composite Plasmonic-Metal/Semiconductor Photoelectrodes: Evidence for Selective Plasmon-Induced Formation of Charge Carriers Near the Semiconductor Surface. *J. Am. Chem. Soc.* **2011**, *14*, 5202–5205.
8. Nagpal, P.; Han, S. E.; Stein, A.; Norris, D. J. Efficient Low-Temperature Thermophotovoltaic Emitters from Metallic Photonic Crystals. *Nano Lett.* **2008**, *8*, 3238–3243.
9. Heine, C.; Morf, R. H. Submicrometer Gratings for Solar Energy Applications. *Appl. Opt.* **1995**, *34*, 2476–2482.
10. Sheng, P.; Bloch, A. N.; Stepleman, R. S. Wavelength-Selective Absorption Enhancement in Thin-Film Solar Cells. *Appl. Phys. Lett.* **1983**, *43*, 579–581.
11. Maier, S. A. *Plasmonics—Fundamentals and Applications*; Springer: New York, 2007.
12. McPheeters, C. O.; Yu, E. T. Computational Analysis of Thin Film InGaAs/GaAs Quantum Well Solar Cells with Back Side Light Trapping Structures. *Opt. Express* **2012**, *20*, 864–878.
13. Landy, N. I.; Sajuyigbe, S.; Mock, J. J.; Smith, D. R.; Padilla, W. J. A. Perfect Metamaterial Absorber. *Phys. Rev. Lett.* **2008**, *100*, 207402.
14. Liu, N.; Mesch, M.; Weiss, T.; Hentschel, M.; Giessen, H. Infrared Perfect Absorber and Its Application as Plasmonic Sensor. *Nano Lett.* **2010**, *10*, 2342–2348.
15. Tittl, A.; Mai, P.; Taubert, R.; Dregely, D.; Liu, N.; Giessen, H. Palladium-Based Plasmonic Perfect Absorber in the Visible Wavelength Range and Its Application to Hydrogen Sensing. *Nano Lett.* **2011**, *11*, 4366–4369.
16. Aydin, K.; Ferry, V. E.; Briggs, R. M.; Atwater, H. A. Broadband Polarization-Independent Resonant Light Absorption Using Ultrathin Plasmonic Super Absorbers. *Nat. Commun.* **2011**, *2*, 517.
17. Hooper, I. R.; Sambles, J. R. Surface Plasmon Polaritons on Narrow-Ridged Short-Pitch Metal Gratings in the Conical Mount. *J. Opt. Soc. Am. A* **2003**, *20*, 836–843.
18. Salamon, Z.; Macleod, H. A.; Tollin, G. Coupled Plasmon-Waveguide Resonators: A New Spectroscopic Tool for Probing Proteolipid Film Structure and Properties. *Biophys. J.* **1997**, *73*, 2791–2797.
19. Salamon, Z.; Tollin, G. Optical Anisotropy in Lipid Bilayer Membrane: Coupled Plasmon-Waveguide Resonance Measurements of Molecular Orientation, Polarizability, and Shape. *Biophys. J.* **2001**, *80*, 1557–1567.
20. Turbadar, T. Complete Absorption of Light by Thin Metal Films. *Proc. Phys. Soc. London* **1959**, *73*, 40–44.
21. Kretschmann, E.; Raether, H. Radiative Decay of Non-Radiative Surface Plasmons Excited by Light. *Z. Naturforsch. A* **1968**, *23*, 2135–2136.
22. Otto, A. Excitation of Nonradiative Surface Plasma Waves in Silver by the Method of Frustrated Total Reflection. *Z. Phys.* **1968**, *216*, 390–410.
23. Faryad, M.; Lakhtakia, A. On Surface Plasmon-Polariton Waves Guided by the Interface of a Metal and a Rugate Filter with a Sinusoidal Refractive-Index Profile. *J. Opt. Soc. Am. B* **2010**, *27*, 2218–2223.
24. Atalla, M. R. M.; Faryad, M.; Lakhtakia, A. On Surface-Plasmon-Polariton Waves Guided by the Interface of a Metal and a Rugate Filter with a Sinusoidal Refractive-Index Profile. Part II: High-Phase-Speed Solutions. *J. Opt. Soc. Am. B* **2012**, *29*, 3078–3086.
25. Faryad, M.; Hall, A. S.; Barber, G. D.; Mallouk, T. E.; Lakhtakia, A. Excitation of Multiple Surface-Plasmon-Polariton Waves Guided by the Periodically Corrugated Interface of a Metal and a Periodic Multilayered Isotropic Dielectric Material. *J. Opt. Soc. Am. B* **2012**, *29*, 704–713.
26. Ferry, V.; Verschuuren, M.; Lare, M. C; Schropp, R. E. I.; Atwater, H. A.; Polman, A. Optimized Spatial Correlations for Broadband Light Trapping Nanopatterns in High Efficiency Ultrathin Film a-SiH Solar Cells. *Nano Lett.* **2011**, *11*, 4239–4245.
27. Bloch, F. Uber die Quantenmechanik der Elektronen in Kristallgittern. *Z. Phys.* **1928**, *52*, 555–600.
28. Ashcroft, N. W.; Mermin, N. D. *Solid State Physics*; Holt Saunders: Philadelphia, 1976; p 113.
29. Moharam, M. G.; Grann, E. B.; Pommet, D. A. Formulation for Stable and Efficient Implementation of the Rigorous Coupled-Wave Analysis of Binary Gratings. *J. Opt. Soc. Am. A* **1995**, *12*, 1068–1076.
30. Dolev, I.; Volodarsky, M.; Porat, G.; Arie, A. Multiple Coupling of Surface Plasmons in Quasiperiodic Gratings. *Opt. Lett.* **2011**, *36*, 1584–1586.
31. Faryad, M.; Lakhtakia, A. Excitation of Multiple Surface-Plasmon-Polariton Waves Using a Compound Surface-Relief Grating. *J. Nanophoton.* **2012**, *6*, 061701.
32. Hall, A. S.; Faryad, M.; Barber, G. D.; Mallouk, T. E.; Lakhtakia, A. Effect of Grating Period on the Excitation of Multiple Surface-Plasmon-Polariton Waves Guided by the Interface of a Metal Grating and a Photonic Crystal. *Proc. SPIE* **2013**, *8620*, 862003.
33. Polo, J. A., Jr.; Mackay, T. G.; Lakhtakia, A. *Electromagnetic Surface Waves: A Modern Perspective*; Elsevier: Waltham, MA, 2013.
34. Nagpal, P.; Lindquist, N. C.; Oh, S. H.; Norris, D. J. Ultrasmooth Patterned Materials for Plasmonics and Metamaterials. *Science* **2009**, *325*, 594–597.